Available online at www.sciencedirect.com
ScienceDirect
International Journal of Heat and Mass Transfer 50 (2007) 4079–4088
International Journal of HEAT and MASS TRANSFER
www.elsevier.com/locate/ijhmt

Thermal blob convection in spherical shells

B. Futterer [a,*], A. Brucks [b], R. Hollerbach [c], C. Egbers [a]

[a] Department of Aerodynamics and Fluid Mechanics, Brandenburg University of Technology Cottbus, Siemens-Halske-Ring 14, 03046 Cottbus, Germany
[b] ZARM, Center of Applied Space Technology and Microgravity, University of Bremen, Am Fallturm, 28359 Bremen, Germany
[c] Department of Applied Mathematics, University of Leeds, Woodhouse Lane, Leeds LS2 9JT, United Kingdom

Received 22 June 2006; received in revised form 20 December 2006
Available online 24 April 2007

Abstract

We present experimental and numerical results on convection of high Prandtl number fluids in a spherical shell of aspect ratio $\beta = (r_o - r_i)/r_i = 1$, with the inner sphere cooled and the outer sphere heated. For sufficiently small Rayleigh numbers the flow is both axisymmetric and steady, consisting of fluid streaming off the south pole of the inner sphere, and returning in the equatorial regions. For larger *Ra* this streaming flow becomes time-dependent, with thermal blobs periodically dripping off the south pole. For even greater *Ra* these pulses become irregular in time. An axisymmetric numerical code is then used to study this phenomenon in more detail. The numerical results agree qualitatively (but not quantitatively) with the experimental results, and suggest furthermore that the transition from regular to irregular behavior may occur via a period-doubling cascade. The numerical code is used to explore the *Pr* and β dependence of this dripping blob phenomenon, and reveals the results to be independent of Prandtl number for $Pr > 100$. In contrast, the aspect ratio plays an important role, with no distinct blobs observed if β is too small.

PACS: 44.25.+f; 47.20.Bp

Keywords: Natural convection; Spherical shells

1. Introduction

Consider a fluid-filled spherical shell, with the inner sphere cooled and the outer sphere heated, and gravity vertically downward. In the 'northern' hemisphere the fluid will be stably stratified, with warm fluid lying above cold. In the 'southern' hemisphere though the situation is reversed, with cold fluid above warm. We would expect therefore that some type of convectively driven flow will be established, acting to transport heat from the outer sphere to the inner. This simple system is thus well suited to studying natural convection and heat transfer, with many of the key results directly transferable to engineering and industrial applications [1–3].

The first experiments on convection in spherical shells were by Scanlan et al. [4–7], who considered a range of aspect ratios $\beta = (r_o - r_i)/r_i$, and found a variety of flow patterns, including crescent and kidney-shaped eddies, as well as so-called falling vortices. Most of these experiments were done using either air or water, having Prandtl numbers $Pr = 0.7$ and 6, respectively. A few experiments were also done using various oils with Prandtl numbers up to 4000, but no detailed flow structures were obtained in these cases. Further experiments using oils with $Pr > 30$ were done by Nakagawa et al. [8] and Egbers et al. [9,10], all in relatively narrow gaps, $\beta \leqslant 0.5$.

Numerical calculations on this problem were done by Garg [11] and Thamire and Wright [12], who succeeded in reproducing many of the experimental results at $Pr = 0.7$ and 6. Large Prandtl numbers were considered by Chu and Lee [13], Chiu and Chen [14], and Wu et al. [3], who focussed more on the initial transients rather than

* Corresponding author. Tel.: +49 355 694893; fax: +49 355 694891.
E-mail address: futterer@tu-cottbus.de (B. Futterer).

0017-9310/$ - see front matter © 2007 Elsevier Ltd. All rights reserved.
doi:10.1016/j.ijheatmasstransfer.2006.12.036

Nomenclature

$\hat{e}_z$	unit vector in the vertical direction
g	acceleration due to gravity
Nu	Nusselt number
P	period
Pr	Prandtl number ν/κ
p	pressure
Ra	Rayleigh number $g\alpha\Delta T(r_o - r_i)^3/\nu\kappa$
r	radial coordinate
r_i	radius of inner sphere
r_o	radius of outer sphere
T	temperature
t	time
$\mathbf{U}$	velocity

Greek symbols

α	thermal expansion coefficient
β	aspect ratio $(r_o - r_i)/r_i$
ΔT	temperature difference
θ	meridional coordinate
κ	thermal diffusivity
ν	kinematic viscosity
ρ	density
τ_{vi}	viscous timescale $(r_o - r_i)^2/\nu$
τ_{th}	thermal timescale $(r_o - r_i)^2/\kappa$
ϕ	azimuthal coordinate
Ψ	streamfunction of $\mathbf{U}$

the final solutions though, and also included features such as taking the inner sphere to be off-center, either raised or lowered relative to the outer sphere.

In this work, we will consider only concentric spheres, concentrating primarily on the relatively wide gap $\beta = 1$, and also on large Pr. We are motivated by the experiments of Brucks [15], who discovered a new type of time-dependent convection, quite distinct from any of the previously known results. In Section 2, we begin by reviewing the basic features of these new convection patterns. In subsequent sections, we then use a numerical code to study these solutions in more detail, and identify the mechanism responsible for the time-dependence. We also map out the range of Prandtl numbers and aspect ratios for which these solutions are observed.

2. Experimental results

Fig. 1 shows a sketch of the experimental apparatus, consisting of an inner aluminium sphere ($r_i = 6$ cm), and an outer acrylic glass sphere ($r_o = 12$ cm), suspended on a vertical central shaft that extends both above and below the inner sphere. The inner sphere's temperature, as cold as 8 °C, is regulated by pumping cold water through the central shaft, and circulating it through the hollow inner sphere. The outer sphere's temperature, as warm as 30 °C, is regulated by pumping warm water through a square tank surrounding the whole apparatus. The temperatures of these two pumping systems were each controlled to an accuracy of 0.3 °C, for an accuracy of 0.5 °C in the temperature difference ΔT.

The fluid filling the spherical gap is a viscous silicone oil having viscosity $\nu \approx 0.1$ cm^2/s and thermal diffusivity $\kappa \approx 10^{-3}$ cm^2/s, for a Prandtl number $Pr = \nu/\kappa \approx 100$. The viscous and thermal timescales are then given by $\tau_{vi} = (r_o - r_i)^2/\nu \approx 6$ min and $\tau_{th} = (r_o - r_i)^2/\kappa \approx 10$ h. One of the questions, we wish to address is which of these two rather different timescales determines the period of our time-dependent solutions.

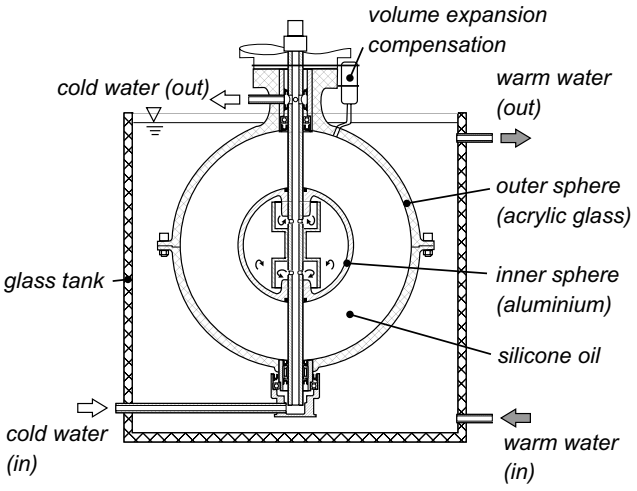

Fig. 1. A sketch of the experimental apparatus.

The flow field was measured using a *Dantec Dynamics* 2D Particle Image Velocimetry (PIV) system; see also [15] for further details of the experimental setup, PIV system, and most of the results. Here, we present just enough of the results to motivate the subsequent numerical work.

As noted above, if the inner sphere is cooler than the outer, the southern hemisphere will be unstably stratified, with cold fluid lying above warm. The induced flow consists of an axisymmetric plume streaming off the south pole of the inner sphere, and returning in the equatorial regions (as in Fig. 3 below). Brucks [15] then found that for sufficiently large Rayleigh numbers, this initially steady plume became time-dependent, with axisymmetric vortex rings periodically dripping off the south pole. Fig. 2 shows one of these periodic solutions. We can see quite clearly how fluid collects in the boundary layer on the inner sphere, and then drips off in a sudden pulse, only to repeat 14 s later. At this Rayleigh number the periodicity is indeed quite regular, but at even larger Ra the pulses become irregular (and considerably faster). Very conveniently, they still

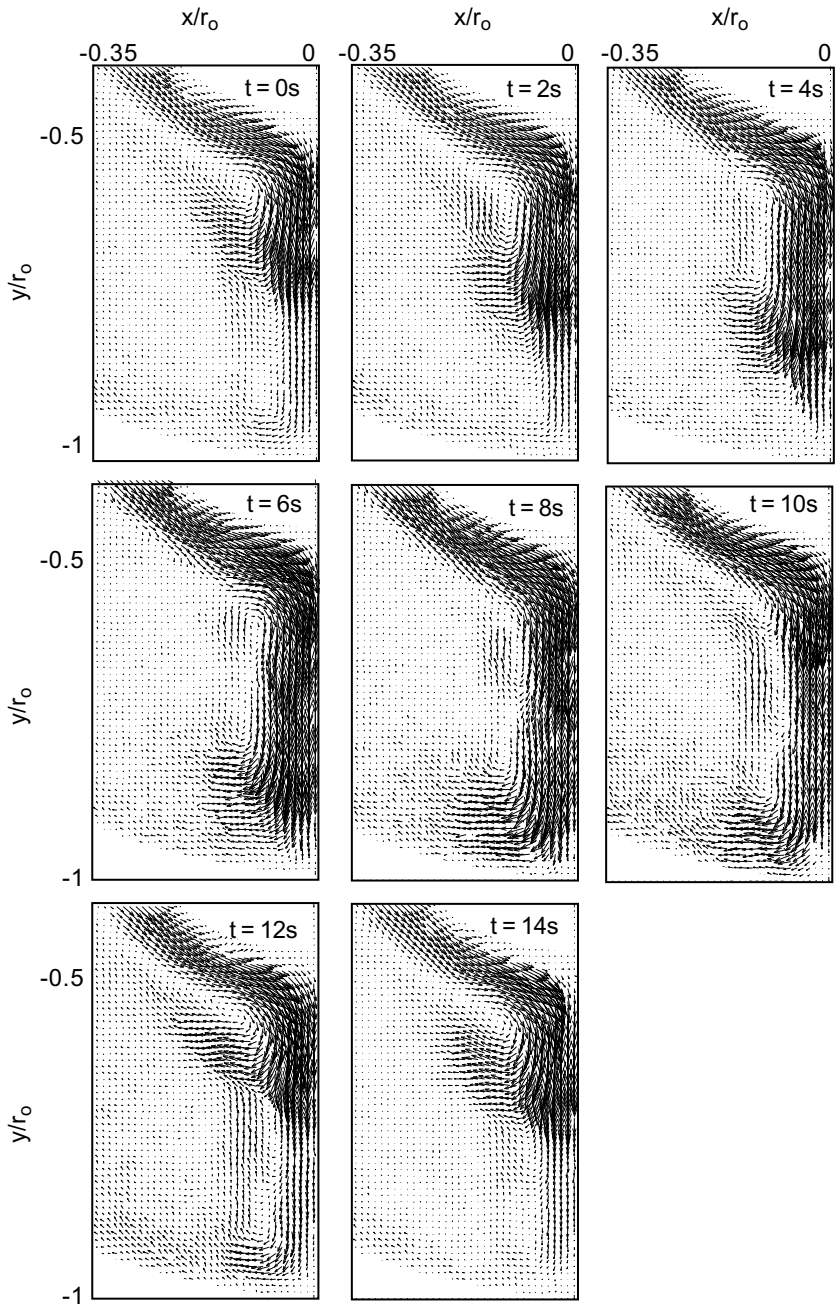

Fig. 2. A sequence of eight PIV measurements, taken at intervals of 2 s. Only the region near the south pole is shown. The maximum velocities are sim20 mm/s. Note, how the flow is virtually the same at $t = 0$ and 14 s. Subsequent pulses then occur with the same periodicity. The Rayleigh number $Ra = 1.4 \times 10^7$. The onset of time-dependence first occurs at $Ra = 7 \times 10^6$.

remain axisymmetric though, greatly facilitating a numerical investigation of this phenomenon.

We emphasize also that these dripping blobs here are very different from the falling vortices referred to above. These occur in much narrower gaps, and consist of a series of vortices that fill the whole gap, and move from the pole to the equatorial regions. (In fact, the way we have formulated the problem, with the inner sphere cooler than the outer, they would be referred to as rising vortices. The original experiments were done with the inner sphere being the warmer one, which interchanges the two hemispheres, thereby yielding falling vortices.)

One last point to note before we consider the problem numerically concerns the limitations of the experimental setup. In particular, we will see that while we obtain excellent qualitative agreement with the basic transition from steady to periodic to chaotic solutions, the critical Rayleigh numbers are an order of magnitude less in the numerics than in the experiment. What could possibly account for such a large discrepancy? We believe the most likely

explanation is this shaft on which the inner sphere is mounted, which unfortunately extends both above and below, precisely where the blobs are forming and dripping off. The disruption that this causes, to both $\mathbf{U}$ and T, is sufficiently great that it could quite plausibly delay the transition to time-dependence by an order of magnitude in Ra. Having a shaft running through the entire apparatus was unfortunately necessary, not just to simplify the inner sphere's cooling circuitry, but also to allow the inner and outer spheres to independently rotate. In fact, neither sphere was rotating for any of the results presented here, but the ability to include rotation was important in other experiments done with the same apparatus. It would certainly be interesting though to repeat the experiments here with a shaft only in the northern hemisphere, and see whether one then obtains quantitative agreement with the numerical results.

3. Equations

Scaling length by the gap width $r_o - r_i$, time by the thermal diffusive timescale $\tau_{th} = (r_o - r_i)^2/\kappa$, $\mathbf{U}$ by $\kappa/(r_o - r_i)$, and T by the imposed temperature difference $\Delta T = T_o - T_i$, the nondimensional equations become

$$\nabla \cdot \mathbf{U} = 0, \tag{1}$$

$$Pr^{-1}\left[\frac{\partial \mathbf{U}}{\partial t} + (\mathbf{U}\cdot\nabla)\mathbf{U}\right] = -\nabla p + \nabla^2\mathbf{U} + RaT\hat{\mathbf{e}}_z, \tag{2}$$

$$\frac{\partial T}{\partial t} + (\mathbf{U}\cdot\nabla)T = \nabla^2 T, \tag{3}$$

where the Prandtl number

$$Pr = \frac{\nu}{\kappa} \tag{4}$$

is a material property of the fluid, and the Rayleigh number

$$Ra = \frac{\alpha \Delta T g (r_o - r_i)^3}{\nu\kappa} \tag{5}$$

measures the imposed thermal forcing. Here ν and κ are the fluid's viscosity and thermal diffusivity, respectively, α is the thermal expansion coefficient, and g is gravity, with $-\hat{\mathbf{e}}_z$ denoting its direction, vertically downward. The boundary conditions associated with (2) are

$$\mathbf{U} = 0 \quad \text{at } r = r_i, r_o, \tag{6}$$

and for (3) they are

$$T = 0 \quad \text{at } r = r_i, \qquad T = 1 \quad \text{at } r = r_o. \tag{7}$$

This system of equations and boundary conditions is solved using the spectral code [16], in which $\mathbf{U}$ and T are expanded in terms of Chebyshev polynomials in r, and Legendre functions in θ. Resolutions as large as 34×250 for $\mathbf{U}$ and 52×400 for T were used, and all results were carefully checked to ensure that they were fully resolved. The code was also benchmarked against the results of Garg [11] and Thamire and Wright [12], with agreement to better than 1%.

Finally, one might wonder why we chose to nondimensionalize on the thermal timescale τ_{th} rather than the viscous timescale τ_{vi}. As we saw above, the experiment has $\tau_{th} \approx 10$ h and $\tau_{vi} \approx 6$ min. Given the dripping period of 14 s, τ_{vi} might then appear to be the more relevant timescale. In fact, by varying the Prandtl number, we will show that the dripping period is determined by τ_{th}, not τ_{vi}. That is, with time nondimensionalized on the thermal timescale, the period of the time-dependent solutions turns out to be independent of Pr, at least for sufficiently large Prandtl numbers.

Indeed, we note that one can set $Pr = \infty$ in (2), and obtain a sensible limit. Eq. (2) is then no longer time-stepped, but becomes instead an elliptic equation, to be inverted at each timestep of (3). Numerically this is quite convenient, as the timestep is then dictated only by (3), and can be considerably larger than if (2) must be time-stepped as well. Physically, setting $Pr = \infty$ corresponds to taking the viscous timescale to be so short that the fluid is assumed to respond instantaneously, that is, $\tau_{vi} = 0$. As we will see below though, even in this limit the period of the time-dependent solutions is exactly the same as it is for large but finite Pr, showing once again that it is τ_{th} rather than τ_{vi} that sets the period.

4. Numerical results

4.1. $\beta = 1$, Steady solutions

Fig. 3 shows solutions for $\beta = 1$, a range of Prandtl numbers from 2 to 100, and Rayleigh numbers from 2×10^5 to 5×10^6. All of these solutions are steady. Note how the flow streams off the south pole, and recirculates in the equatorial regions. The resulting circulation cell is precisely one of these kidney-shaped eddies referred to above. For larger Ra, it no longer really resembles a kidney though. Instead, the flow becomes increasingly concentrated in thin boundary layers at the inner and outer spheres. Similarly, the plume descending from the south pole also becomes increasingly concentrated right on the axis. (It is at this point that we realize just how disruptive the shaft in the experiment really is; without it this descending plume would be much more strongly focussed on the axis.)

Turning next to the region above the inner sphere, it is indeed almost completely stationary, as we would expect a stably stratified region to be. In fact, there is a very weak counter-rotating circulation cell in this region, indicated by the dotted contour line. These small counter-rotating cells have previously also been obtained by Garg [11], but are so weak that they almost certainly have no influence on the rest of the flow. Finally, we note the very narrow thermal boundary layer just above the inner sphere.

4.2. $\beta = 1$, Periodic solutions

As indicated in Fig. 3, steady solutions no longer exist if Pr and Ra are sufficiently large. Fig. 4 shows which types of

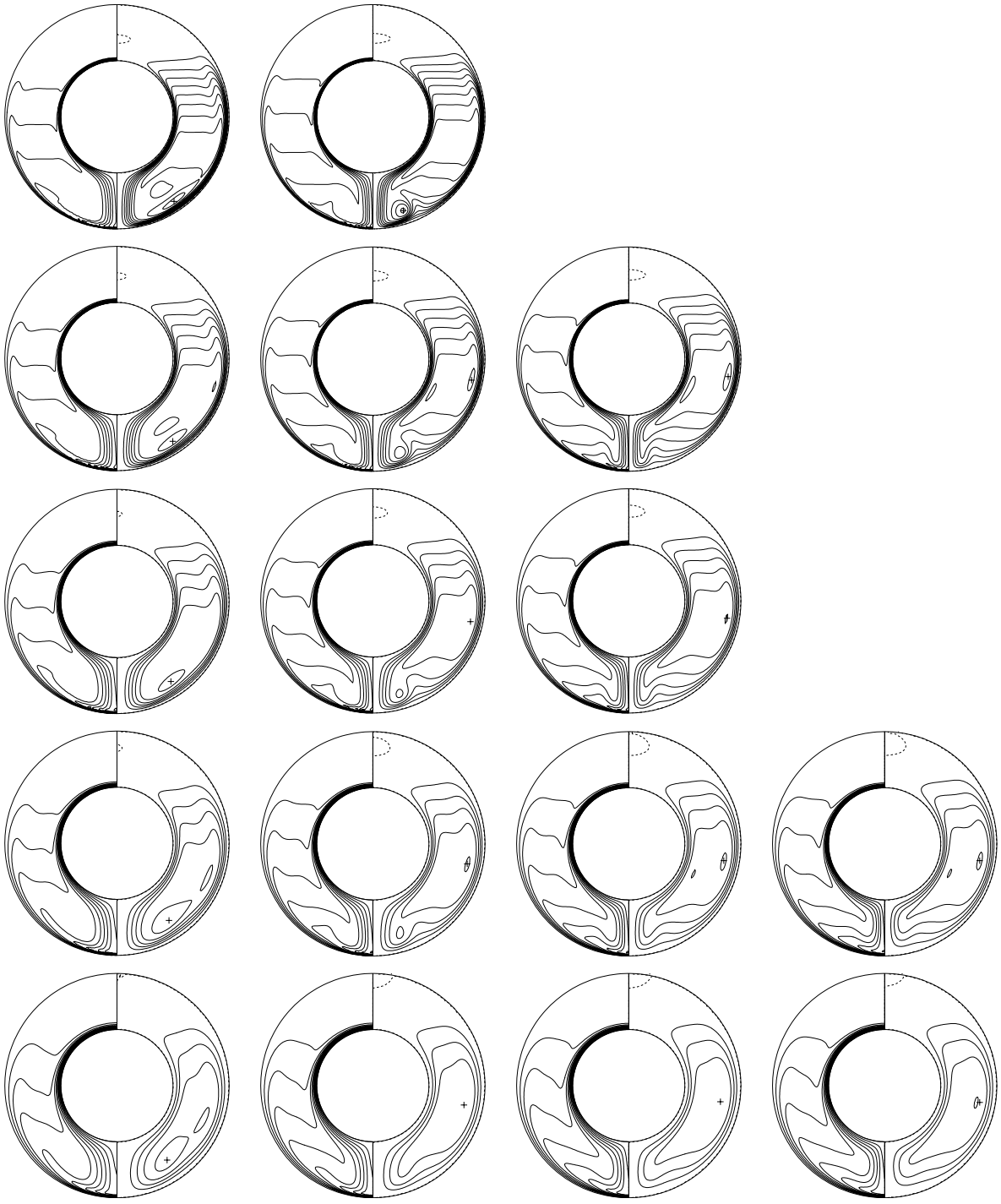

Fig. 3. From left to right $Pr = 2$, 6, 25 and 100; from bottom to top $Ra = 2 \times 10^5$, 5×10^5, 1×10^6, 2×10^6 and 5×10^6. Within each panel the left half shows the temperature, varying between 0 on the inner sphere and 1 on the outer; the right half shows the streamfunction of the flow, with the + indicating the maximum. The four blank panels in the top right corner correspond to (Pr, Ra) combinations for which the solutions are no longer steady; what happens in this region will be considered in Section 4.2.

solutions exist in different parts of the (Pr, Ra) parameter space. For $Pr = 100$ the critical Rayleigh number for the onset of time-dependent solutions is $Ra_c = 8 \times 10^5$ (for comparison, we recall that in the experiment we had $Ra_c = 7 \times 10^6$). For $Pr > 100$ we have $Ra_c = 6 \times 10^5$, essentially independent of Pr. In contrast, for $Pr < 100$, Ra_c increases quite dramatically, until for $Pr \leqslant 10$ no time-dependent solutions were found at all, even for Ra as large as 10^7. This presumably explains why these solutions have not been obtained before; most previous work has concentrated on relatively small Prandtl numbers, where these new solutions do not exist.

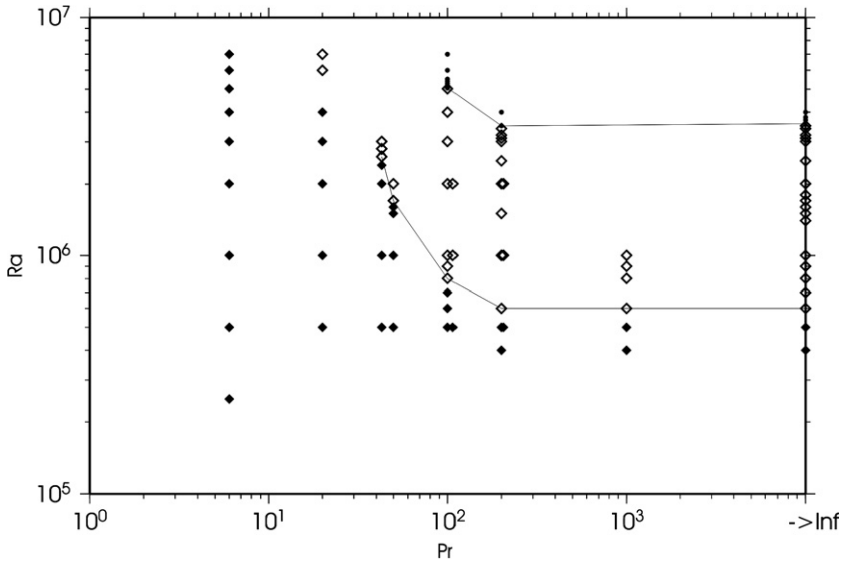

Fig. 4. The onset of time-dependence as a function of Prandtl number. ♦ indicates steady solutions, ◇ indicates periodic solutions, and ● indicates irregularly fluctuating solutions. The solid lines denote the critical Rayleigh numbers for the transitions from steady to periodic to irregular.

Fig. 5 shows an example of one of these new periodic solutions, at $Pr = \infty$ and $Ra = 10^6$ (so about 50% greater than Ra_c). In the first panel, the solution looks much like the ones in Fig. 3. As time progresses though, by the fourth panel we see the gradual development of a separate little circulation cell at the inner sphere's south pole. This vortex reaches its maximum strength in the fifth panel, where we also begin to see it dripping off the south pole. In the remaining three panels, it is then swept along until it merges again with the main, kidney-shaped circulation. Despite the rather different values of Ra_c, it is thus clear that this is essentially the same dripping blob phenomenon as in Fig. 2.

The period of this solution in Fig. 5 is $P = 0.00104$, that is, roughly 1/1000 of the thermal diffusive timescale τ_{th} on which we nondimensionalized. For comparison, in the experiment we had 14 s/10 h = 1/2600. Given the considerable discrepancies in Ra_c, we could hardly expect better agreement in the periods. So, what causes the time-dependence in the first place, and why is it such a small fraction of τ_{th}? Evidently each new blob must lose a certain amount of heat to the inner sphere before it can drip off; the natural timescale is then the diffusive timescale across the thermal boundary layer, which is indeed a small fraction of τ_{th}. See also Howard [17], Krishnamurti [18], and Clever and Busse [19,20], who study similar thermal blobs in plane

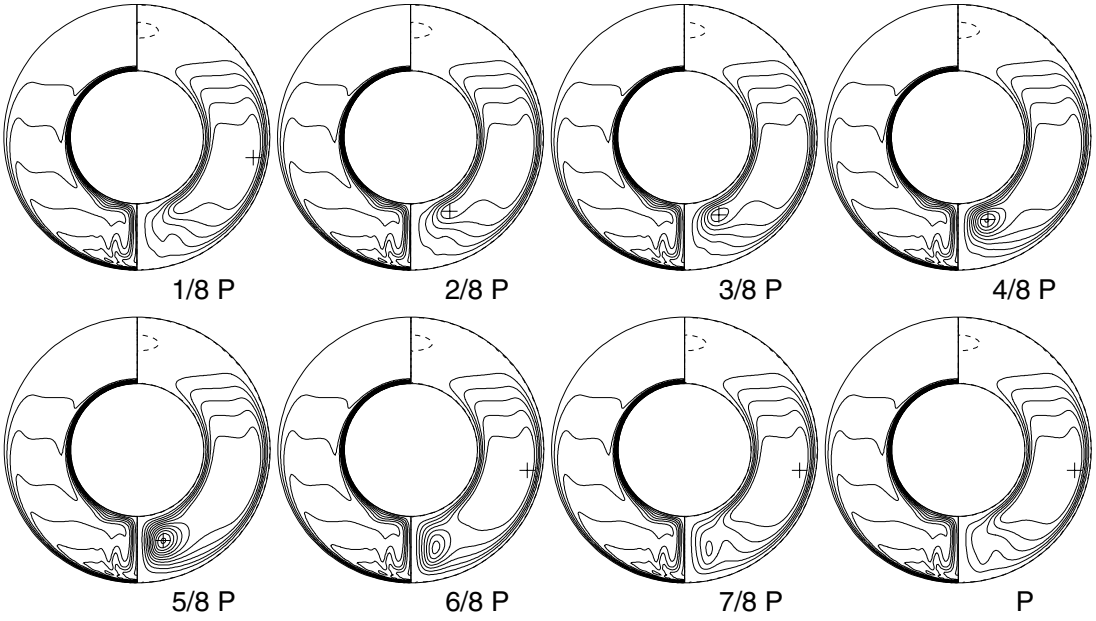

Fig. 5. Eight uniformly spaced snapshots of the periodic solution at $\beta = 1$, $Pr = \infty$ and $Ra = 10^6$. The period $P = 0.00104$. As in Fig. 3, the left half of each panel shows the temperature, and the right half the streamfunction of the flow.

layer convection, and also find that the period is consistently a small fraction of τ_{th}.

4.3. $\beta = 1$, Period-doubled solutions

Returning once more to Fig. 4, we recall that there is a further transition from periodic to irregular solutions. This was studied in some detail for $Pr = \infty$, and found to consist of at least two period-doubling bifurcations, before the actual transition to irregular behavior. Fig. 6 shows the effect of these period-doublings, occurring at $Ra = 1.7 \times 10^6$ and 3.1×10^6, respectively. The first panel in each row show how the maximum of the streamfunction Ψ_{max} varies in time. We can clearly see how each individual dripping blob corresponds to a sudden pulse in Ψ_{max}; note in particular in Fig. 5 how Ψ_{max} is located within the blob

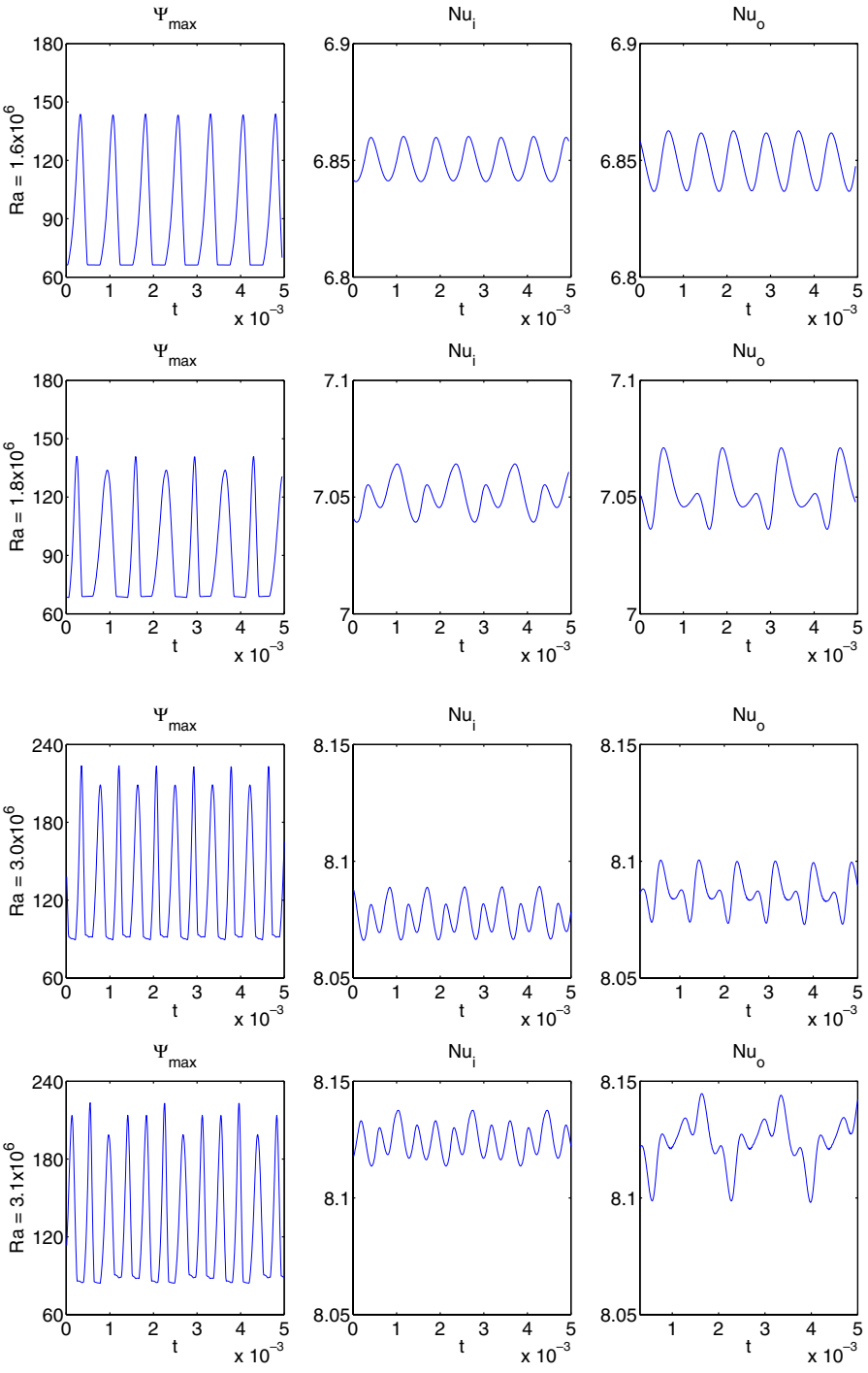

Fig. 6. From top to bottom, the four rows are at $Ra = 1.6 \times 10^6$, 1.8×10^6, 3.0×10^6 and 3.1×10^6. The first two rows therefore indicate the effect of the first period-doubling, the second two rows the second period-doubling. Within each row the three panels show Ψ_{max}, Nu_i and Nu_o as functions of t.

when it is most strongly developed, but within the main kidney-shaped eddy between pulses. The period doublings then correspond to slight variations in the strengths of successive dripping blobs. Their spatial structure is virtually unaffected by the period-doublings though.

The second and third panels show the Nusselt number, evaluated at the inner and outer boundaries. The Nusselt number is defined as

$$Nu = \int\int \frac{\partial T}{\partial r} \mathrm{d}S \Big/ \int\int \frac{\partial T_0}{\partial r} \mathrm{d}S, \tag{8}$$

where the integrals are evaluated over either the inner or the outer boundaries (the integration over ϕ is of course redundant here), and T_0 is the temperature distribution one would obtain if there were no flow, that is, it is the solution of the problem $\nabla^2 T_0 = 0$, $T_0(r_\mathrm{i}) = 0$, $T_0(r_\mathrm{o}) = 1$.

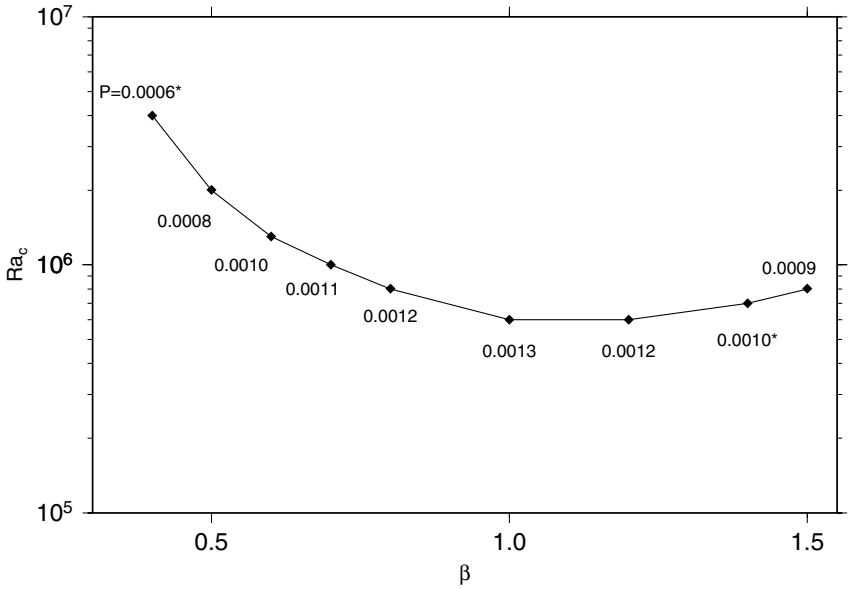

Fig. 7. The dependence on β of Ra_c, the critical Rayleigh number for the onset of time-dependence. $Pr = \infty$. The numbers beside individual points indicate the periods P of the corresponding solutions.

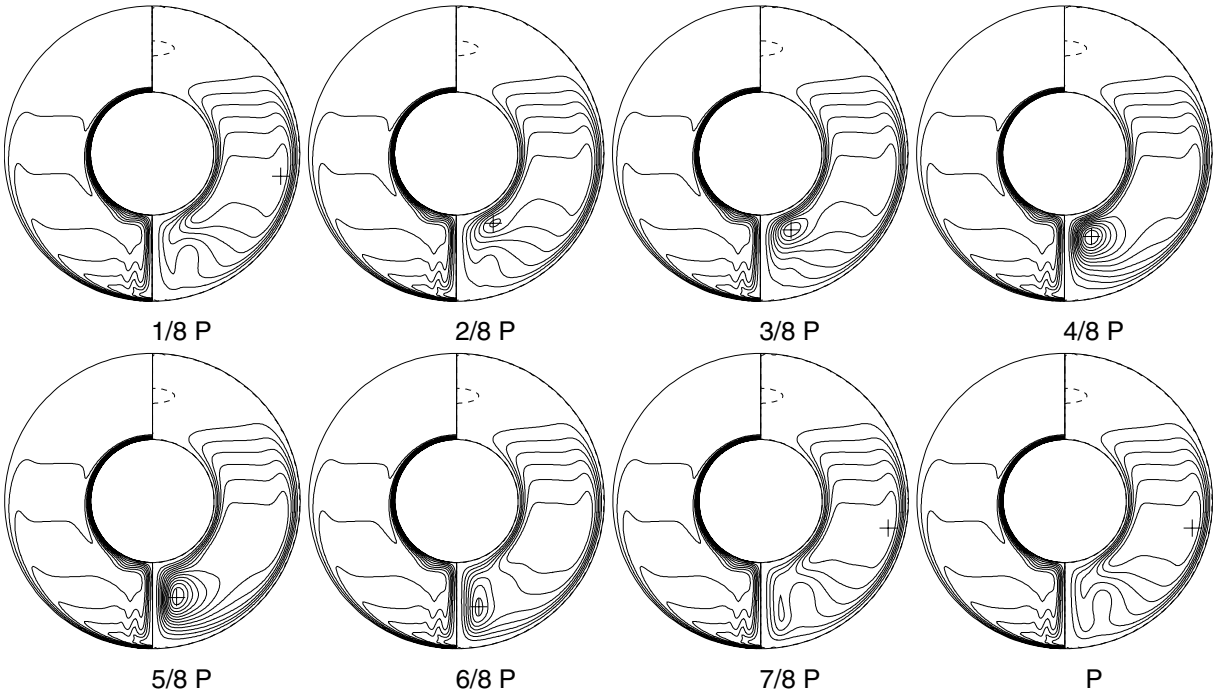

Fig. 8. Eight uniformly spaced snapshots of the periodic solution at $\beta = 1.4$, $Pr = \infty$ and $Ra = 7 \times 10^5$. The period $P = 0.00096$. As in Fig. 3, the left half of each panel shows the temperature, and the right half the streamfunction of the flow.

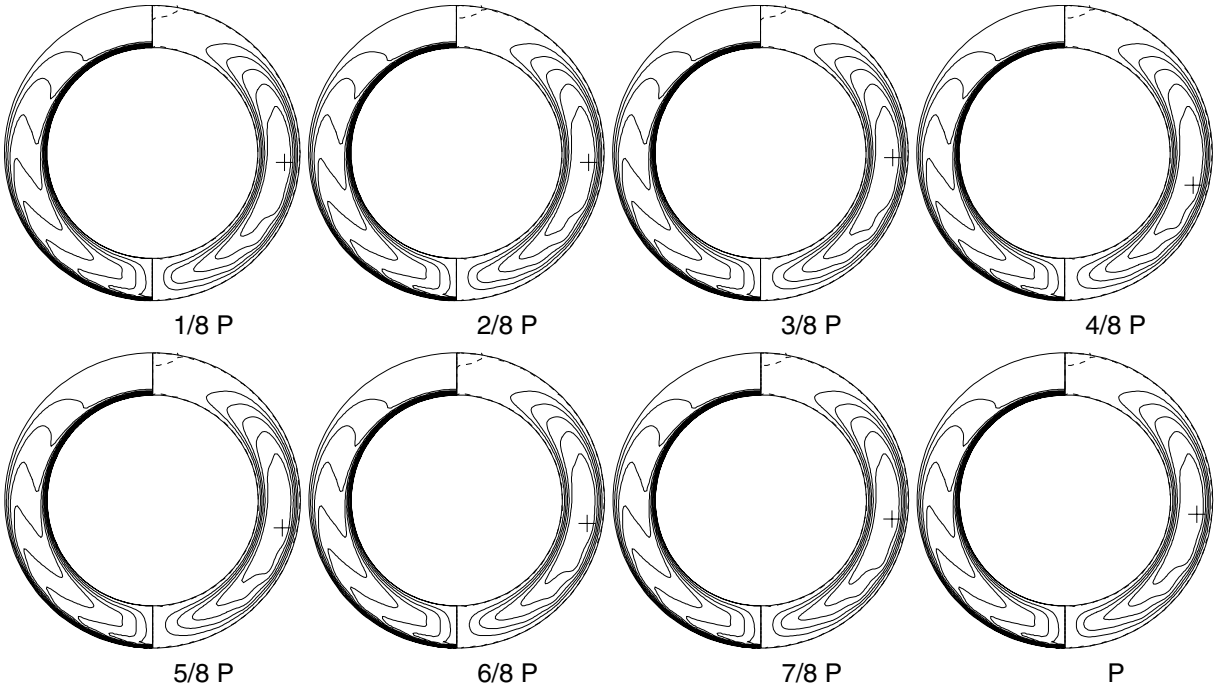

Fig. 9. Eight uniformly spaced snapshots of the periodic solution at $\beta = 0.4$, $Pr = \infty$ and $Ra = 4 \times 10^6$. The period $P = 0.00064$. As in Fig. 3, the left half of each panel shows the temperature, and the right half the streamfunction of the flow.

Nu therefore measures the ratio of the actual heat flux to what one would obtain by pure conduction, in the absence of convection. For steady solutions, one must of course have $Nu_i = Nu_o$, but for time-dependent solutions only their time-averages must be equal. We see then that each dripping blob also causes a pulse in the heat flux, and that the period-doublings again show up as variations in strength.

Another point to note about Fig. 6 is that – leaving aside the period-doublings – the frequency of individual pulses increases with increasing Ra. At the initial onset, at $Ra_c = 6 \times 10^5$, we have $P = 0.0013$, whereas at $Ra = 3.7 \times 10^6$ we have $P = 0.0004$. We recall that the same reduction in P was found in the experiment as well. The likeliest explanation for this reduction in P is that as Ra is increased, the thickness of the thermal boundary layer decreases (Fig. 3), so the relevant timescale also decreases.

Finally, for $Ra > 3.7 \times 10^6$ the flow becomes irregular, with no definite periodicity. Given the two previous period-doublings, one might conjecture that this is due to a period-doubling cascade to chaos, but the calculations were far too time-consuming to verify this. For the same reason, we were also not able to verify whether the solutions for $Ra > 3.7 \times 10^6$ are chaotic at all, or merely quasi-periodic.

4.4. Varying β

All of the preceding results have been at $\beta = 1$. The reason for this was of course the original experiment [15]. It would nevertheless be of interest to vary β as well, and see how this dripping blob phenomenon is altered. To keep the computational effort affordable, all of these calculations were done at $Pr = \infty$ only. Fig. 7 shows how the critical Rayleigh number for the onset of time-dependence varies with β. It is interesting to note that the original $\beta = 1$ yields the lowest Ra_c.

Figs. 8 and 9 show the time-dependent solutions at $\beta = 1.4$ and 0.4, respectively. Turning to the wider gap first, we see the blobs dripping off just as in Fig. 5. In contrast, in the narrower gap the nature of the time-dependence has changed, and now consists merely of rather subtle fluctuations in the details of the flow. Presumably a $\beta = 0.4$ gap is simply too narrow for proper vortices to form, which most likely also explains why Ra_c increases rather steeply for decreasing β.

5. Conclusion

In this work, we have presented a new type of time-dependent solution in natural convection between concentric spherical shells. We showed that this dripping blob phenomenon is controlled by the thermal diffusive timescale, in particular by the diffusion of heat across the inner thermal boundary layer, similar to previous results in plane layer convection [17–20]. We mapped out the range of Prandtl numbers and aspect ratios for which this phenomenon exists, and found that it disappears if either Pr or β becomes too small. Indeed, it would be quite interesting to map out the entire (β, Pr, Ra) parameter space, and see whether these thermal blob solutions are connected in any way with the previously known falling vortex solutions (for example).

Classifying how all the various solutions depend on (β, Pr, Ra) would be computationally very challenging though, even for an axisymmetric problem such as this.

Acknowledgements

This work was supported by the German Federal Ministry of Education and Research, through the German Aerospace Center e.V. (DLR), Grant No. FKZ 50 WM0122. The experimental apparatus used here was funded by German Science Foundation (DFG) under Grant No. EG 100/1.

References

[1] A. Laouadi, M. Atif, Natural convection heat transfer within multilayer domes, Int. J. Heat Mass Transfer 44 (10) (1981) 1973–1981.
[2] D. Flowers, K. Anderson, Numerical simulation of conduction heat transfer in a system of slowly rotating concentric spheres, Numer. Heat Transfer Part A 46 (2004) 851–863.
[3] H. Wu, W. Tsai, H. Chou, Transient natural convection heat transfer of fluids with variable viscosity between concentric and vertically eccentric spheres, J. Heat Mass Transfer 47 (2004) 1685–1700.
[4] E. Bishop, L. Mack, J. Scanlan, Heat transfer by natural convection between concentric spheres, Int. J. Heat Mass Transfer 9 (1966) 649–662.
[5] J. Scanlan, E. Bishop, R. Powe, Natural convection heat transfer between concentric spheres, Int. J. Heat Mass Transfer 13 (1970) 1857–1872.
[6] S. Yin, R. Powe, J. Scanlan, E. Bishop, Natural convection flow patterns in spherical annuli, Int. J. Heat Mass Transfer 16 (1973) 1785–1795.
[7] R. Powe, R. Warrington, J. Scanlan, Natural convective flow between a body and its spherical enclosure, Int. J. Heat Mass Transfer 23 (1980) 1337–1350.
[8] T. Nakagawa, J. Zierep, K. Bühler, M. Wimmer, K. Kirchartz, Thermal convection between two concentric spheres, in: Proceedings of the Second JSME-KSME Thermal Engineering Conference, October 12–21, 1992, pp. 13–18.
[9] C. Egbers, Zur Stabilität der Strömung im konzentrischen Kugelspalt, Dissertation, ZARM, Universität Bremen, 1994.
[10] C. Egbers, W. Beyer, H. Rath, LDV-Measurement on thermal convective instabilities in spherical gap flow, in: Proceedings of the 8th International Symposium on Applications of Laser Techniques to Fluid Mechanics, July 8–11, 1996, Lisbon, Portugal, pp. 23.4.1–23.4.8.
[11] V. Garg, Natural convection between concentric spheres, Int. J. Heat Mass Transfer 35 (1992) 1935–1945.
[12] C. Thamire, N. Wright, Multiple and unsteady solutions for buoyancy driven flows in spherical annuli, Int. J. Heat Mass Transfer 41 (1998) 4121–4138.
[13] H. Chu, T. Lee, Transient natural convection heat transfer between concentric spheres, J. Heat Mass Transfer 36 (1993) 3159–3170.
[14] C. Chiu, W. Chen, Transient natural convection heat transfer between concentric and vertically eccentric spheres, J. Heat Mass Transfer 39 (1996) 1439–1452.
[15] A. Brucks, Untersuchungen zur thermischen Konvektion im weiten Kugelspalt mit und ohne Rotation, Diplomarbeit, ZARM, Universität Bremen, 2000.
[16] R. Hollerbach, A spectral solution of the magneto-convection equations in spherical geometry, Int. J. Numer. Meth. Fluids 32 (2000) 773–797.
[17] L. Howard, Convection at high Rayleigh number, in: Proceedings of the 11th International Congress on Applied Mechanics, 1966, pp. 1109–1115.
[18] R. Krishnamurti, On the transition to turbulent convection. Part 2. The transition to time-dependent flow, J. Fluid Mech. 42 (1970) 309–320.
[19] R. Clever, F. Busse, Steady and oscillatory bimodal convection, J. Fluid Mech. 271 (1994) 103–118.
[20] R. Clever, F. Busse, Standing and travelling oscillatory blob convection, J. Fluid Mech. 297 (1995) 255–273.